Cylindrical vector beam rotary Nd:YAG disk laser with birefringent crystal

Sanbin Chen (陈三斌)[1,*], Jianlang Li (李建郎)[2], and Ken-Ichi Ueda[3]

[1]*National Key Laboratory on Solid-State Laser, Beijing 100015, China*
[2]*University of Shanghai for Science and Technology, Shanghai 200093, China*
[3]*Institute for Laser Science, University of Electro-Communications, Tokyo 182-8585, Japan*
**Corresponding author: chensanbin@aliyun.com*

Received May 25, 2020; accepted August 18, 2020; posted online October 22, 2020

A rotating neodymium-doped yttrium aluminum garnet (Nd:YAG) disk laser resonator for efficiently generating vector beams with azimuthal and radial polarization is demonstrated. In the study, the laser crystal rotary for thermal alleviation and polarization discrimination uses *c*-cut ytterbium vanadate (YVO_4). The laser output could be switched between azimuthal and radial polarizations by simply adjusting the cavity length. The laser power reached 4.38 W and 4.64 W for azimuthally and radially polarized beams at the slope efficiencies of 45.3% and 48.5%, respectively. Our study proved that an efficient, high-power vector rotary disk laser would be realistic.

Keywords: cylindrical vector beam; rotary disk; polarization.
doi: 10.3788/COL202018.121401.

Cylindrical vector beams (CVBs) with axial polarization symmetry are of particular importance for a variety of applications and have attracted lots of interest in the past decades. The radial and azimuthal polarizations in them can be focused tightly and form strong longitudinal electric or magnetic fields at the focal spot. So, they are widely used in material processing, particle trapping and acceleration, high-resolution microscopy[1–7], and so on.

Azimuthally or radially polarized beams have been created in many ways, either by extra-cavity optics or intracavity elements. The former mainly focuses on the spatial transformation of a linearly or circularly polarized beam into a radially or azimuthally polarized beam by using various converters[8–11]. The latter denotes the oscillation of the eigen vector mode forced by various polarization-selective elements[12–16] inside the laser resonator. However, among various vectors, the thermal deposition in the solid-state gain medium similarly obstructs further power scaling with high beam quality[17]. To alleviate the thermal effect, the thin-disk geometry and an intra-cavity circular resonant waveguide grating were adopted for vector mode oscillation and had shown the ability of kilowatt (kW)-level output[18,19]. Nevertheless, being a sub-wavelength structure with concentric and multilayer corrugation, the waveguide grating mirror is sensitive to lasing wavelength, and also its fabrication mentions so-called auto-cloned technology[18], which undoubtedly renders this element costly.

Therefore, it is necessary to develop alternative technology with cost advantage and ability of power scalability to produce vector polarized beams. To eliminate the thermal effect, in present years, the rotating disk technology, proposed by Basu[20], became another way to manipulate the thermal deposition in gain media. This technology uses the mechanical rotation of gain medium to remove the deposited thermal load outside the cavity to dissipate thermally[20–24], which exhibits the merits in enabling the high-power and single-mode laser and outputs covering the infrared, visible, and UV regions[25].

Among the various polarization selectors ever reported, the birefringent crystal is with low-cost and available everywhere, and the spatial walk-off along with it provides us with a simple and efficient discrimination mechanism for cylindrical vector modes in a wide range of wavelengths. We have demonstrated the generation of the radially and azimuthally polarized laser beams in the same laser by using a *c*-cut ytterbium vanadate (YVO_4) crystal, and there are two ways to realize the conversion between two kinds of vector polarized beams[26]. Comparing with the previous work using a rotary disk neodymium-doped yttrium aluminum garnet (Nd:YAG) crystal as a gain medium, in this study, an improvement of the power efficiency was achieved. Both the radially and azimuthally polarized outputs are obtained in a laser. The detailed results of our study are given as follows.

The experimental setup of our laser is schematically illustrated in Fig. 1. The laser resonator is a plano-concave straight running cavity, which consists of a plano-concave mirror with 50 mm curvature radius (HR), a Nd:YAG disk, two intra-cavity lenses with respective focal lengths

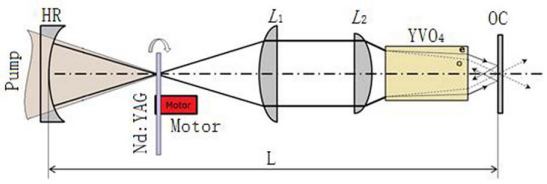

Fig. 1. Experimental setup of the rotary laser with the axis-symmetrical walk-off effect.

of 50 mm (L_1) and 40 mm (L_2), a *c*-cut YVO_4, and the flat–flat output coupler (OC) coating with 90% reflectivity at 1064 nm. The gain medium had a dimension of $\Phi 50 \times 1.5$ mm and 1.0 at.% doping concentration of neodymium ions whose two surfaces were anti-reflection (AR) coated at 808 nm and 1064 nm. The HR is a dichroic mirror whose plane surface was AR coated at 808 nm, and the concave surface was AR coated at 808 nm and high-reflection coated at 1064 nm. The pump source is a fiber coupled 808 nm laser diode, and its pigtail fiber has a 400 μm core diameter and a numerical aperture of 0.22. The pump radiation was focused by a coupler (1:1) in the sample along the cavity axis. The converging pump light passed through HR into a 600 μm spot size and illuminated on the disk. The disk was rotated by a controllable speed motor in between two cooling plates. Heat is removed from the heat disk by conduction across the gas gap between the disk and the heat sink. The disk was in the middle of the HR and L_1 in the cavity. The distance between HR and L_1 was 100 mm. Plane and convex surfaces of L_1 and L_2 were AR coated at 1064 nm, and the distance between them was 40 mm. The OC was behind L_2, and it could be one dimensionally moved along the cavity axis at a minimum step of 10 μm. With such a setup, there were two beam waists formed in this cavity, and one waist was at the position of the laser crystal, while the other one was on the surface of the OC.

In this cavity, the 8 mm × 8 mm × 20 mm YVO_4 crystal whose two end surfaces were AR coated at 1064 nm was between L_2 and OC as the polarization element. Owing to the positive birefringence of the YVO_4 crystal, the forward light coming from the L_2 side is separated into the extraordinary and ordinary wave components (e and o rays), and then they would converge at different points along the cavity axis. When the OC was at one of the converging points of either the e ray or o ray, the corresponding ray component would be formed in the round-trip in the resonator.

In the beginning of the experiment, the crystal disk was driven to rotate at a specific rotation rate (R_r) of 3 Hz, and, as Fig. 1 shows, the OC near YVO_4 was placed close to the position of the estimated converging point of the o ray. At the absorbed pump power (P_{abs}) above 2 W, the OC was moved, and the laser would begin to oscillate in doughnut-shaped mode when the OC was in the right position. Thereafter, the laser cavity was adjusted to maximize the output power corresponding to the OC on an optimum position.

The output power of the laser showed the dependences on both P_{abs} and R_r. Figure 2 plots the function relation between the output power and R_r when P_{abs} varied. As seen in each curve, when the pump power was fixed at one specific level, the output powers of the laser increased and then decreased with R_r, and their respective maxima appeared at an optimal rotation rate of R_r within a range of 4–6 Hz. For example, at $P_{abs} = 10.72$ W, the laser power increased slowly with R_r before reaching its maximum of 4.38 W at $R_r = 5.6$ Hz and then decreased with R_r. At

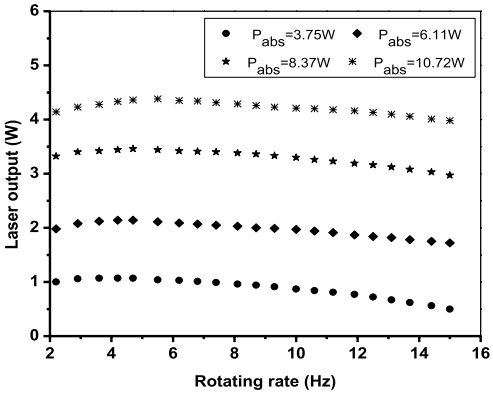

Fig. 2. Output power of rotary disk laser versus rotation rate at different pump powers.

small values of R_r, the increases of laser power with R_r were mainly attributed to a quick shift of the thermal loading out of the excitation region, owing to the mechanical rotation, the thermal diffusion in the laser crystal's volume, and also the thermal convection between the crystal's surface and the cooling air fluid. Nevertheless, when R_r exceeded the optimum rotation rate, the sweeping time of pump light for a cycle became comparable with or smaller than the ~230 μs upper-level lifetime of the Nd^{3+} ion in the YAG crystal, thus the stored energy in Nd^{3+} ion could not be extracted efficiently[27], and also the waste heat produced in the crystal could not dissipate effectively during each cycle of the rotation, which degraded the laser output power.

According to Fig. 2, at one specific rotation rate R_r, the output power increased with the pump power. To be clear, Fig. 3 illustrates the laser power as a function of absorbed pump power at the optimum rotation rate $R_r = 5.6$ Hz of this laser. Herein, the laser had a threshold pump power around $P_{abs} = 1.68$ W, and its output power increased linearly with pump power and reached 4.38 W at $P_{abs} = 10.72$ W with slope efficiency of $\eta_{se} = 45.3\%$.

The profile of the laser beam was monitored by a CCD camera. It was observed that the laser oscillated in

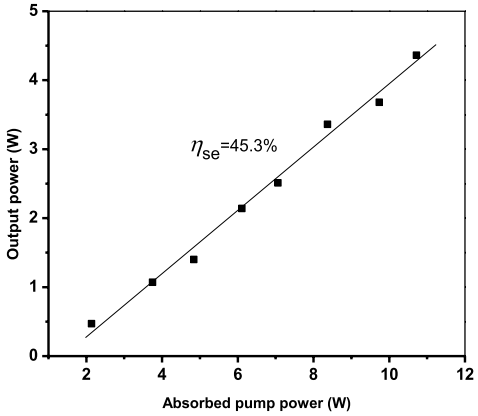

Fig. 3. Laser output power versus absorbed pump power at $R_r = 5.6$ Hz.

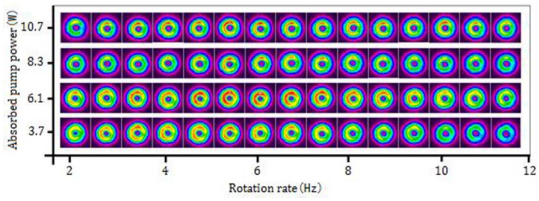

Fig. 4. Variations of far-field intensity distribution of laser beams with rotation rates at different pump powers.

doughnut-shaped mode. Figure 4 depicts the captured intensity distributions of the laser beam when both rotation rate and pump power varied. As illustrated, when the rotation rate of the disk increased from 2 Hz to 12 Hz, the laser beams obtained at four different pump powers ($P_{\mathrm{abs}} = 3.75$ W, 6.11 W, 8.37 W, and 10.72 W) always exhibited annular intensity patterns with respective central nulls. This result indicated that the transverse mode pattern of this laser could be maintained well when the pump power and rotation rate varied.

Further, the polarization state of the obtained laser mode was checked by using a linear polarizer as the analyzer. For the laser beam obtained at $P_{\mathrm{abs}} = 10.72$ W and optimum rotation rate, Figs. 5(a)–5(d) plot their intensity distributions transmitted through the polarizer analyzer while the analyzer was rotated at different orientations. As seen, each transmitted intensity profile showed central-symmetrical two-lobe structures, with their respective direction perpendicular to the corresponding polarizer axis. This result manifested that the doughnut-shaped laser mode obtained from this rotary disk laser was azimuthally polarized.

In the step described above, the OC was close to the YVO_4 crystal, and azimuthally polarized laser output was obtained. In subsequent work, the OC was moved away from the YVO_4 crystal and located at the estimated converging point of the e ray, and the OC was adjusted to another doughnut-shaped laser mode oscillator and then was placed in the optimal position, where maximized output power can be obtained.

Further, when the pump power was set at one specific value above the lasing threshold, the function relation between the output power and the rotation rate was similar to that described in Fig. 2. Specifically, at $P_{\mathrm{abs}} = 10.72$ W, the laser power increased slowly with R_r before reaching the maximum of 4.64 W at $R_r = 5.6$ Hz and then decreased with R_r. Figure 6 plots the laser's output power

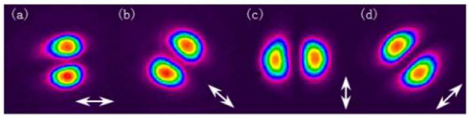

Fig. 5. Far-field intensity distributions of the laser beam (when OC was close to YVO_4 and doughnut-shaped mode was output, $P_{\mathrm{abs}} = 10.72$ W) transmitted through the polarizer analyzer when the polarizer was rotated, where the white arrows indicate the corresponding axis of the polarizer.

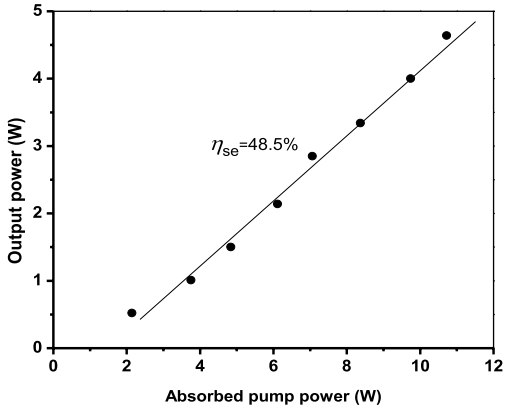

Fig. 6. Output power of the rotating disk laser versus the absorbed pump power at $R_r = 5.6$ Hz.

as a function of pump power at $R_r = 5.6$ Hz. As shown, at $R_r = 5.6$ Hz, the laser has a threshold pump power of $P_{\mathrm{abs}} = 1.68$ W, and its output power increased linearly with the pump power at a slope efficiency of $\eta_{\mathrm{se}} = 48.5\%$ and reached 4.64 W at $P_{\mathrm{abs}} = 10.72$ W.

Worthwhile to point out, the doughnut-shaped intensity distribution of the laser mode was kept at different pump powers and rotation rates. Figure 7 depicts variation of the intensity distributions of laser beam with the pump power at the optimum rotation rate, and it was clear that the laser beam exhibited the annular intensity distribution with a dark center when the pump powers varied from 4.84 W to 10.72 W.

Similarly, the polarization state of the obtained laser beams was also checked. Figure 8 shows the far-field intensity distributions of the beam profile transmitted through the linear polarization analyzer at $R_r = 5.6$ Hz and $P_{\mathrm{abs}} = 10.72$ W. As seen, the two-lobe structure in each image was parallel to the polarizer axis. This means that the local polarization state of the off-axis lobe was parallel

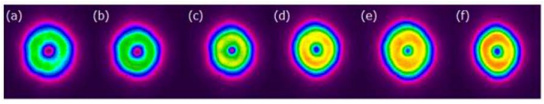

Fig. 7. Variations of far-field intensity distribution of the laser beam with pump power at $R_r = 5.6$ Hz: (a) $P_{\mathrm{abs}} = 4.84$ W, (b) $P_{\mathrm{abs}} = 6.11$ W, (c) $P_{\mathrm{abs}} = 7.07$ W, (d) $P_{\mathrm{abs}} = 8.37$ W, (e) $P_{\mathrm{abs}} = 9.74$ W, and (f) $P_{\mathrm{abs}} = 10.72$ W, respectively.

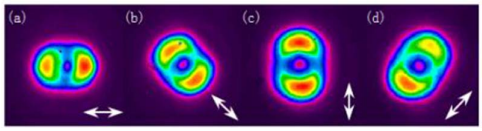

Fig. 8. Far-field intensity distributions of the laser beam (when OC was far away from YVO_4 and doughnut-shaped mode was output, $P_{\mathrm{abs}} = 10.72$ W) transmitted through the polarizer analyzer when the polarizer was rotated, where the white arrows indicate the corresponding axis of the polarizer.

to the direction of the corresponding polarizer axis, namely, identical to the axial direction of itself. Therefore, the laser beam was a radially polarized beam.

It should be emphasized that the transverse intensity profiles of the obtained radially and azimuthally polarized beams did not show substantial change at any of the rotation rates and pump power above the lasing threshold, and there was no need to insert an aperture into laser cavity to suppress the other mode oscillation at high pump power. The mode stabilities of the obtained vector beams in this experiment were very high and were not disturbed by the mechanical noise commonly generated in rotary disks and laboratories.

In summary, for the first time, to the best of our knowledge, vector modes with azimuthal and radial polarizations were produced in a rotary disk laser, and this laser was efficient and stable. In the study, the rotary disk geometry of the laser gain medium was adopted to alleviate thermal deposition inside the excitation region, and a birefringent crystal was used to discriminate the oscillation of different vector modes. The results of this study revealed that the rotary disk laser is valuable for the generation of high-power vector modes.

The author S. Chen thanks Prof. Anhan Liu for fruitful discussions and technical support on the rotating disk crystal and acknowledges Prof. Xiaojun Tang, Prof. Hong Zhao, and Prof. Shouhuan Zhou for helpful discussions.

References

1. V. G. Niziev and A. V. Nesterov, J. Phys. D **32**, 1455 (1999).
2. Q. Zhan, Opt. Express **12**, 3377 (2004).
3. J. Fontana and R. Pantell, J. Appl. Phys. **54**, 4285 (1983).
4. S. Deng, Y. Xiao, J. Hu, J. Chen, Y. Wang, and M. Liu, Chin. Opt. Lett. **16**, 111801 (2018).
5. Y. Zhang and J. Bai, Opt. Express **17**, 3698 (2009).
6. Z. Y. Gu, X. H. Wang, J. X. Wang, F. Fan, and S. J. Chang, Chin. Opt. Lett. **17**, 121103 (2019).
7. S. Quabis, R. Dorn, M. Eberler, O. Glöckl, and G. Leuchs, Opt. Commun. **179**, 1 (2000).
8. S. C. Tidwell, G. H. Kim, and W. D. Kimura, Appl. Opt. **32**, 5222 (1993).
9. C. Y. Han, Z. H. Wei, Y. Hsu, K. H. Chen, C. H. Yeh, W. X. Wu, and J. H. Chen, App. Sci. **6**, 241 (2016).
10. T. Grosjean, D. Courjon, and M. Spajer, Opt. Commun. **203**, 1 (2002).
11. Y. Q. Zhang, X. Y. Zeng, R. R. Zhang, Z. J. Zhan, X. Li, L. Ma, C. X. Liu, C. W. He, and C. F. Cheng, Opt. Lett. **43**, 4208 (2018).
12. Z. Bozmon, G. Biener, V. Kleiner, and E. Hasman, Opt. Lett. **27**, 285 (2002).
13. J. L. Li, K. Ueda, M. Musha, A. Shirakawa, and L. X. Zhong, Opt. Lett. **31**, 2969 (2006).
14. H. Kawauchi, Y. Kozawa, and S. Sato, Opt. Lett. **31**, 2151 (2006).
15. I. Moshe, S. Jackel, and A. Mier, Opt. Lett. **28**, 807 (2003).
16. T. Moser, M. A. Ahmed, F. Pigeon, O. Parriaux, E. Wyss, and T. Graf, Laser Phys. Lett. **1**, 234 (2004).
17. J. L. Li, K. Ueda, M. Musha, L. X. Zhong, and A. Shirakawa, Opt. Lett. **33**, 2686 (2008).
18. M. A. Ahmed, M. Haefner, M. Vogel, C. Pruss, A. Voss, W. Osten, and T. Graf, Opt. Express **19**, 5093 (2011).
19. D. Tom, R. Martin, B. Frieder, M. Cherry May, P. Christof, O. Wolfgang, A. A. Marwan, and G. Thomas, Opt. Lett. **43**, 1371 (2018).
20. S. Basu and R. L. Byer, Appl. Opt. **29**, 1765 (1990).
21. S. Basu, M. Camargo, and J. Donnelly, Proc. SPIE **5075**, 251 (2005).
22. S. M. Massey, J. B. McKay, T. H. Russell, A. H. Paxton, H. C. Miller, and S. Basu, J. Opt. Soc. Am. B **22**, 1003 (2005).
23. A. P. Ongstad, M. Guy, and J. R. Chavez, Opt. Express **24**, 108 (2016).
24. S. Basu, Proc. SPIE **6871**, 68710N (2008).
25. J. Korn, T. H. Jeys, and T. Y. Fan, Opt. Lett. **16**, 1741 (1991).
26. S. Chen, J. Li, S. Zhou, H. Zhao, and K. Ueda, Opt. Express **27**, 15136 (2019).
27. J. L. Li, K. Ueda, L. X. Zhong, M. Musha, A. Shirakawa, and T. Sato, Opt. Express **16**, 10841 (2008).